ELSEVIER

Journal of Structural Geology 30 (2008) 664–681

JOURNAL OF STRUCTURAL GEOLOGY

www.elsevier.com/locate/jsg

Stratigraphic versus structural control on the deformation pattern associated with the evolution of the Mt. Catria anticline, Italy

S. Tavani [a,*], F. Storti [a], F. Salvini [a], C. Toscano [b]

[a] *Dipartimento di Scienze Geologiche, Università degli studi ''Roma Tre'', Rome, Italy*
[b] *E&P Division, ENI S.p.A., San Donato Milanese, Italy*

Received 1 March 2007; received in revised form 29 January 2008; accepted 30 January 2008
Available online 8 February 2008

Abstract

The evolution of deformation patterns during thrust-related folding is of importance for both industrial and academic purposes because of the control that it exerts on the migration and accumulation of fluids in reservoirs. The link between structural position and deformation pattern has been described in both theoretical and field works. On the other hand, the well-documented dependence of deformation structures on the mechanical rock properties and on the environmental conditions indicates that, during folding, structural, stratigraphic, and environmental variables interact to control the deformation pattern within folds. In this work we describe the deformation pattern of the Mt. Catria anticline (Northern Apennines, Italy) and we investigate its variability with (1) the across-strike structural position, and (2) the rock type in the same structural position. Point (1) allowed us to identify and use the syn-folding deformation structures to constrain the fold kinematics. The result of point (2) analyses allowed us to divide the exposed Umbro-Marchean multilayer into three major mechanical units characterised by specific deformation mechanisms and patterns.

Keywords: Thrust-related folding; Brittle deformation analysis; Mechanical stratigraphy; Cross-section balancing; Northern Apennines

1. Introduction

Fold kinematics play a primary role in determining the type, frequency, and attitude of folding-related deformation structures in fault-related folds (e.g. Dahlstrom, 1990; Fischer et al., 1992; Storti and Salvini, 1996; Cardozo et al., 2005; Tavani et al., 2006a). These deformation structures in turn exert a first-order influence on the migration and accumulation of fluids in reservoirs within thrust wedges (e.g. Cooper, 1992; Gholipour, 1998; Van Dijk et al., 2000). Because of this, a variety of studies have attempted to provide criteria for predicting folding-related deformation patterns from numerical (e.g. Erickson and Jamison, 1995; Strayer and Suppe, 2002; Salvini and Storti, 2004), analogue (e.g. Chester et al., 1991), and geometrical (e.g. Sanderson, 1982; Hedlund et al., 1994; Storti and Salvini, 1996; Salvini and Storti, 2001) modelling. These studies suggested that structural (i.e. geometrical and kinematical) variables control the final deformation pattern in the fold. Accordingly, its study can provide an additional tool for constraining the kinematics of natural folds (e.g. Thorbjornsen and Dunne, 1997). On the other hand, the well-documented dependence of folding-related deformation structures on the mechanical stratigraphy (e.g. Corbett et al., 1987; Woodward and Rutherford, 1989; Protzman and Mitra, 1990; Gross, 1995; Couzens and Wiltschko, 1996; Fischer and Jackson, 1999; Chester, 2003; Di Naccio et al., 2005) and environmental conditions (e.g. pressure, temperature, water circulation) during folding (e.g. Chester et al., 1991; Jamison, 1992; Lemiszki et al., 1994), indicates that the study of deformation pattern must also include stratigraphic and environmental variables.

In this paper, we describe the structural and stratigraphic influences on the deformation pattern in the Mt. Catria anticline

* Corresponding author: Departament de Geodinamica i Geofisica, Facultat de Geologia, Universitat de Barcelona, c/ Marti Franques s/n, 08028 Barcelona, Spain. Tel.: +34 93 403 5957.
E-mail address: stefano.tavani@ub.edu (S. Tavani).

0191-8141/$ - see front matter © 2008 Elsevier Ltd. All rights reserved.
doi:10.1016/j.jsg.2008.01.011

of the Northern Apennines and we use the deformation pattern distribution to constrain the fold kinematic evolution.

2. Geological setting of the Mt. Catria anticline

The Mt. Catria anticline is located in the external sector of the Northern Apennines (Fig. 1a) and has been site of many structural studies (e.g. Alvarez et al., 1978; Marshak et al., 1982; Geiser, 1988; Barchi et al., 1991; Chilovi et al., 2002; Massoli et al., 2006). It formed in Messinian times, when the area was incorporated in the Apenninic thrust wedge (e.g. Elter et al., 1975; Bigi et al., 1989). The stratigraphic succession involved in the Mt. Catria anticline consists of four major mechanical units (Fig. 1b): (1) a Triassic thick sequence of alternating of dolostones, anhydrites and limestones (*Anidridi di Burano* Formation and *Calcari ad Rhaetavicula Contorta* Formation); (2) lower Jurassic, poorly layered platform limestones (*Calcare Massiccio* Formation); (3) a lower Jurassic–Miocene pelagic sequence including mainly well-bedded limestones, marly limestones and marls (form *Corniola* to *Bisciaro* Formations); (4) a Miocene to Pliocene siliciclastic sequence consisting of mainly sandstones and marls (*Schlier* and *Marnoso Arenacea* Formations) (e.g. Centamore et al., 1972, 1975). In the study area, the Liassic to Lower Cretaceous succession is characterised by eteropies and lateral thickness variations resulting from a complex palaeobathymetry produced by the Liassic extensional tectonics associated to the Tethian rifting (e.g. Alvarez, 1989; Santantonio, 1993; Marchegiani et al., 1999). The complete ''classical'' Umbro-Marchean multilayer is exposed in the central fold sector (Fig. 1) (Centamore et al., 1972, 1975), where we performed our structural study (Fig. 2). We did so to avoid additional structural complexities associated with the reactivation of inherited Jurassic faults, which has been described in the northern and southern parts of the structure (e.g. Chilovi et al., 2002).

A seismic profile passing through the Mt. Catria anticline and intersecting the ''Burano 1'' well (line PS-338-85) was made available by ENI S.p.A. for this study. Line PS-338-85 allowed us to identify the main deep features of the structure (Fig 3a), which include, below the anticline, a major forethrust and two backthrusts. Steeply dipping reflectors below the Mt. Catria forethrust possibly relate to lower Jurassic normal faults. The central part of the presented segment of line PS-338-85 strikes near parallel to the periclinal hinge of the thrust-related fold immediately to the west of the Mt. Catria anticline. This implies that the imaged TWT outline of the former fold is strongly distorted.

In the study area, the Mt. Catria anticline trends NW–SE, and exhibits a concentric geometry, where no discrete hinge zones can be traced between the crest and the fold limbs (Fig. 3b). Bedding dip across the fold strike progressively passes from 60° toward the SW in the southwestern sectors, and up to 90° in the northeastern sector, where beds are locally overturned. The leading syncline is tight and, in the southern sector, its axial surface is reactivated as a second order thrust (Figs. 1 and 3). The trailing syncline is characterised by second order faulting and folding in the hangingwall of a thrust flat located within the *Scaglia Cinerea* Formation (e.g. De Feyter and Menichetti, 1986). The ''Burano 1'' well encountered the *Calcare Massiccio* Formation up to a depth of 305 m, followed by the *Calcari a Rhaetavicula Contorta* Formation (50 m), and by the *Anidriti di Burano* Formation down to the well bottom (2178 m b.s.l.) (Martinis and Pieri, 1964). In the Umbro-Marchean area, the lower part of the *Anidridi di Burano* Formation has been drilled in the ''Perugia 2'' well (Fig. 1) where the computed thickness of the formation is about 1400 m. The last 350 m of the formation include alternating anhydrites and shales and, in the lower part, shales that overly the *Verrucano* Formation (Martinis and Pieri, 1964). The stratigraphy of the ''Perugia 2'' well is assumed in this paper as representative of the deeper multilayer sector of the Mt. Catria area (Fig. 1b). In this sector of the Apennines, the *Anidriti di Burano* Formation provides the most efficient décollement layer (e.g. Bally et al., 1986; De Feyter and Menichetti, 1986; Calamita et al., 1991; Menichetti et al., 1991; Anelli et al., 1994).

The balanced cross section of the Mt. Catria anticline (Fig. 3b) assumes, coherently with field observation (see below), area preservation in the layers stratigraphically below the *Bosso/Calcari diasprini* Formation. This implies bed thickness and line-length preservation in the *Corniola* and *Calcare Massiccio* Formations, and only area preservation in the ''ductile'' *Anidridi di Burano* Formation (Fig. 3b). Under these assumptions, the detachment depth can be estimated (e.g. Chamberlin, 1910) and would locate within the *Anidridi di Burano* Formation, and in particular about 1050 m below its top. This level locates at the transition between the carbonatic/dolomitic/anydritic and the anhydritic/clayish portion of the *Anidridi di Burano* Formation.

3. Structural data

Structural data on faults, tectonic pressure solution cleavages, joints, and veins were collected at 122 georeferenced field analysis sites in the Mt. Catria anticline (Fig. 2a). This high field sites number allowed us to provide a representation of the deformation pattern at the fold scale, reducing the influence of local distributions.

We identified in the field solution cleavages, veins, joints, and faults (Figs. 4 and 5). Furthermore, we collected data on fractures of uncertain attribution. These elements are classified as: (1) uncertain joints/veins when their attribution is uncertain but, in the same field site, they are parallel to joint/vein sets; (2) generic fractures when their attribution is uncertain and cannot be inferred. We did so that later we could use precise geometric criteria to discriminate joint and vein from faults without mesoscopic evidence of slip (e.g. Tavani et al., 2006a). Structural data were collected in the *Calcare Massiccio*, *Corniola*, *Maiolica*, and *Scaglia* Formations. The first two formations are exposed in the crestal sector of the anticline, whereas the latter are exposed in the steeply dipping limbs. The *Maiolica* Formation is exposed all along the fold (Figs. 1–3). For each structure we collected data on its orientation,

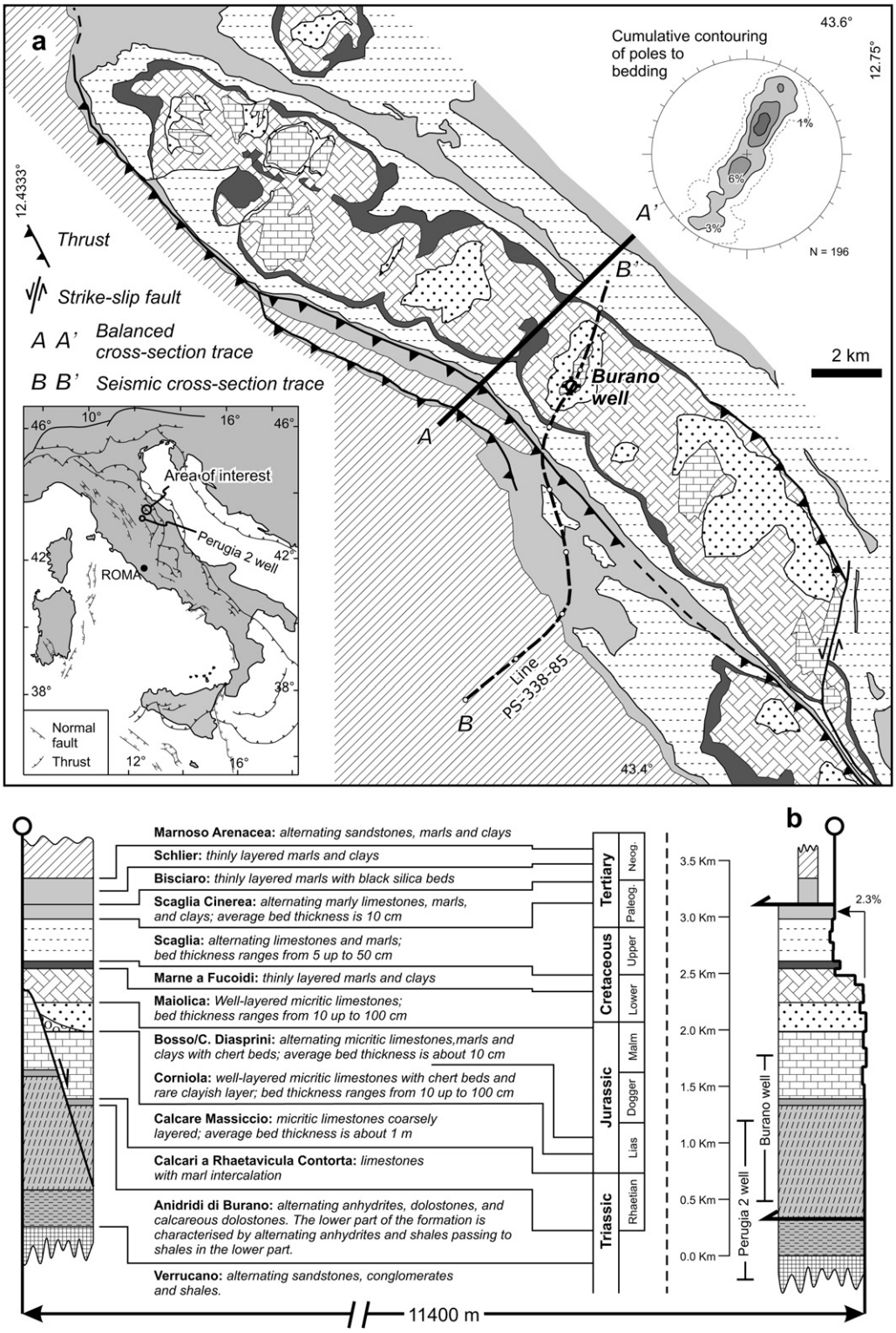

Fig. 1. (a) Geological map of Mt. Catria anticline area (after Centamore et al., 1972, 1975). (b) Stratigraphic succession in the Mt. Catria anticline area and line-length restoration (from the *Verrucano* to the *Scaglia Cinerea* Formations) of the balanced cross-section of Fig. 3b.

overprinting relationships, spacing (the distance between adjacent surfaces, S), termination or non-termination at bedding, and angle to bedding (ATB). Data about constantly spaced stratabound structures include thickness of the boundary layers (H) to normalise their spacing by computing the H/S ratio, which is numerically equivalent to the C/B fissility of Durney and Kisch (1994).

The first phase of our investigation was a geometric analysis of the present and unfolded geometry of all the mesostructures we observed (Tavani et al., 2006a). Structures were

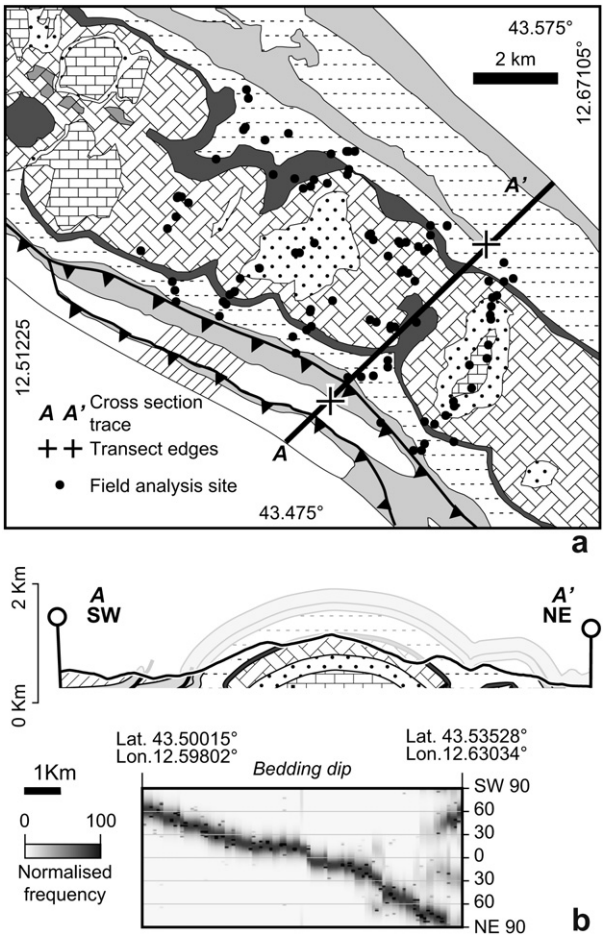

Fig. 2. (a) Field sites distribution in the study area with cross-section and transect traces. (b) Transect analysis showing the variability of bedding dip across the fold and comparison with cross-section. The smoothed and filtered parameter frequency is shown in grey tones (see Salvini et al., 1999 for details). Points correspond to original data.

classified as longitudinal, transverse, or oblique with respect to the fold axis trend (e.g. Stearns, 1968; Hancock, 1985; Cooper, 1992) and divided into subsets. The mean orientation and standard deviation are computed according to the method of Mardia (1972). In the following analyses, to discriminate different subsets, polymodal distributions are interpreted as the sum of N wrapped normal distributions (e.g. Fraser and Suzuki, 1966; Wise et al., 1985; Salvini et al., 1999; Storti et al., 2006). This choice is dictated by the fact that analyses are performed on data collected at different sites. The procedure we followed for data unfolding (Ramsay, 1967) only partially reduces this spatial variability, since it does not allow us to restore rotations along the axis perpendicular to bedding. Accordingly, the wrapped normal distribution does not imply any physical assumption, but has to be regarded to as the simplest choice. Moreover, it is supported by the fact that, when applied to unimodal distributions, it provided satisfying fits (see below).

We investigated the across strike spatial variability of deformation structure attributes by using structural transects (e.g. Wise and McCrory, 1982; Salvini et al., 1999; Tavani et al., 2004). Here we project the position of field sites onto a section line and plot various structural parameters as the *y*-variable along the transect (Fig. 2b). Comparison of cumulative and transect statistical analyses, supported by overprinting relationships observed in the field, allows us to interpret the relative timing of each mesostructure with respect to folding (i.e. pre-, syn- and post-folding). Deformation structures are identified as syn-folding when their attributes are characterised by a spatial variability that is coherent with the fold geometry.

In the second phase of our analysis, syn-folding deformation structures are extracted from the dataset and the corresponding subsets (faults, pressure solution surfaces, joints/veins) are statistically analysed along structural transects to identify homogeneously deformed fold sectors. Finally, in the third step, specific subsets are created for each sector, and statistically analysed by cumulative and spatial (structural transects) diagrams to obtain the within-sector variability of deformation structures (Tavani et al., 2006a).

3.1. Fault data

Small-scale faults are abundant in the Mt. Catria anticline, both as layer-parallel shear surfaces and deformation structures at a high angle to bedding (Fig. 4). In their present orientation (i.e. unrotated analysis), poles to fault surfaces are clustered around two broad maxima corresponding to roughly N–S and, above all, roughly E–W striking surfaces (Fig. 6a). The corresponding rotated analysis is characterised by a major maximum, corresponding to bedding-parallel faults, and by two subordered and broadly distributed maxima corresponding to roughly E–W and N–S striking surfaces. Fault slickenlines are quite scattered both in the unrotated and in the rotated analysis (Fig. 6b). Three broad maxima can be identified and correspond to roughly E–W, N–S, and NE–SW slip directions. The cumulative analysis of fault rotaxes (i.e. the line lying on the fault surface and orthogonal to slickenlines; Wise and Vincent, 1965) exhibits a lower data scattering with respect to those of the poles to faults and slickenlines. Rotaxes are clustered in two well-defined maxima: (1) near vertical and (2) sub-horizontal NW–SE striking (i.e. parallel to the fold axis) rotaxes (Fig. 6c). In the rotated analysis, data scattering increases and a third broad and subordered maximum occurs, corresponding to roughly NE–SW striking sub-horizontal rotaxes.

To analyse the fault data in detail, we divided the dataset into subsets according to the rotax plunge, the best-clustered fault attribute. The rotax plunge in the rotated analysis (Fig. 7a) is roughly symmetrically distributed with respect to the 0° (i.e. horizontal rotaxes). This distribution, more than that in the unrotated analysis (characterised by a higher standard deviation), allows us to divide the fault population into subsets. In particular, the rotated rotax plunge distribution is characterised by a polymodal distribution that we interpret as the sum of three wrapped (circular range is π) normal distributions. The main peak in the frequency diagram (Fig. 7a) corresponds to sub horizontal rotaxes, whereas the other two peaks are roughly symmetric with respect to the mean peak,

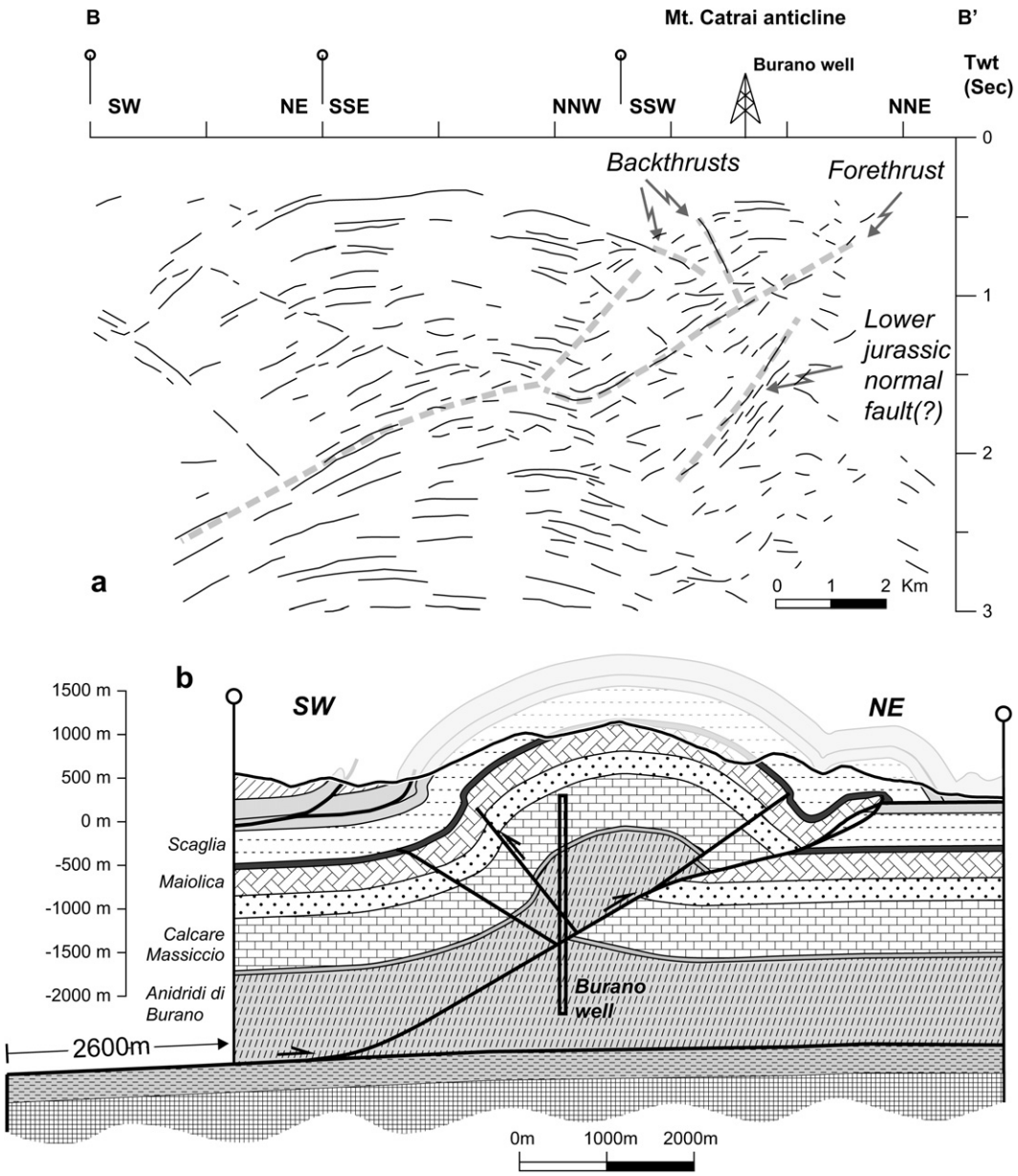

Fig. 3. (a) Line-drawing of the seismic line PS-338-85 (horizontal scale approximately equal to vertical scale). (b) Balanced cross-section across the central sector of the Mt. Catria anticline (see Fig. 1 for location).

and include faults with rotaxes at a high angle to bedding. Accordingly, faults can be divided into two subsets: faults with rotaxes sub-parallel to the corresponding bedding surface (set A), and faults with rotaxes at a high angle to the corresponding bedding surface (subset B), i.e. strike–slip faults (Fig. 7b). Poles to right-lateral strike–slip fault surfaces of subset B define two maxima including N–S striking surfaces (I) and NE–SW striking surfaces (II) (Fig. 7c). Poles to left-lateral strike–slip fault surfaces of subset B define two subsets striking ENE–WSW (III) and ESE–WNW (IV), respectively. Analysis of rotated slickenline plunge of subset A faults defines two maxima; the first one includes faults with shallowly dipping slickenlines (subset A1), whereas the second one includes faults with steeply dipping slickenlines (subset A2) (Fig. 7d). Subset A1 corresponds to fault surfaces parallel to bedding whose movement direction defines three maxima (Fig. 7e): the first one (V) includes fault slickenlines orthogonal to the fold axial trend; the second and third maxima include slip directions roughly parallel to those of subsets (I) and (III). These faults are layer parallel steps of subsets (I) and (III) faults and, accordingly, are associated with them (Fig. 8). The residual dataset (subset A2) is characterised by a scattered slickenline strike distribution that can be divided into two broadly distributed subsets corresponding to slip directions ranging from 0°N and 90°E (set VI) and from 90°W to 0°N (set VII) (Fig. 7e). The dip of faults belonging to subset VI, both in the rotated and in the unrotated analysis, shows a rather symmetric distribution with respect to

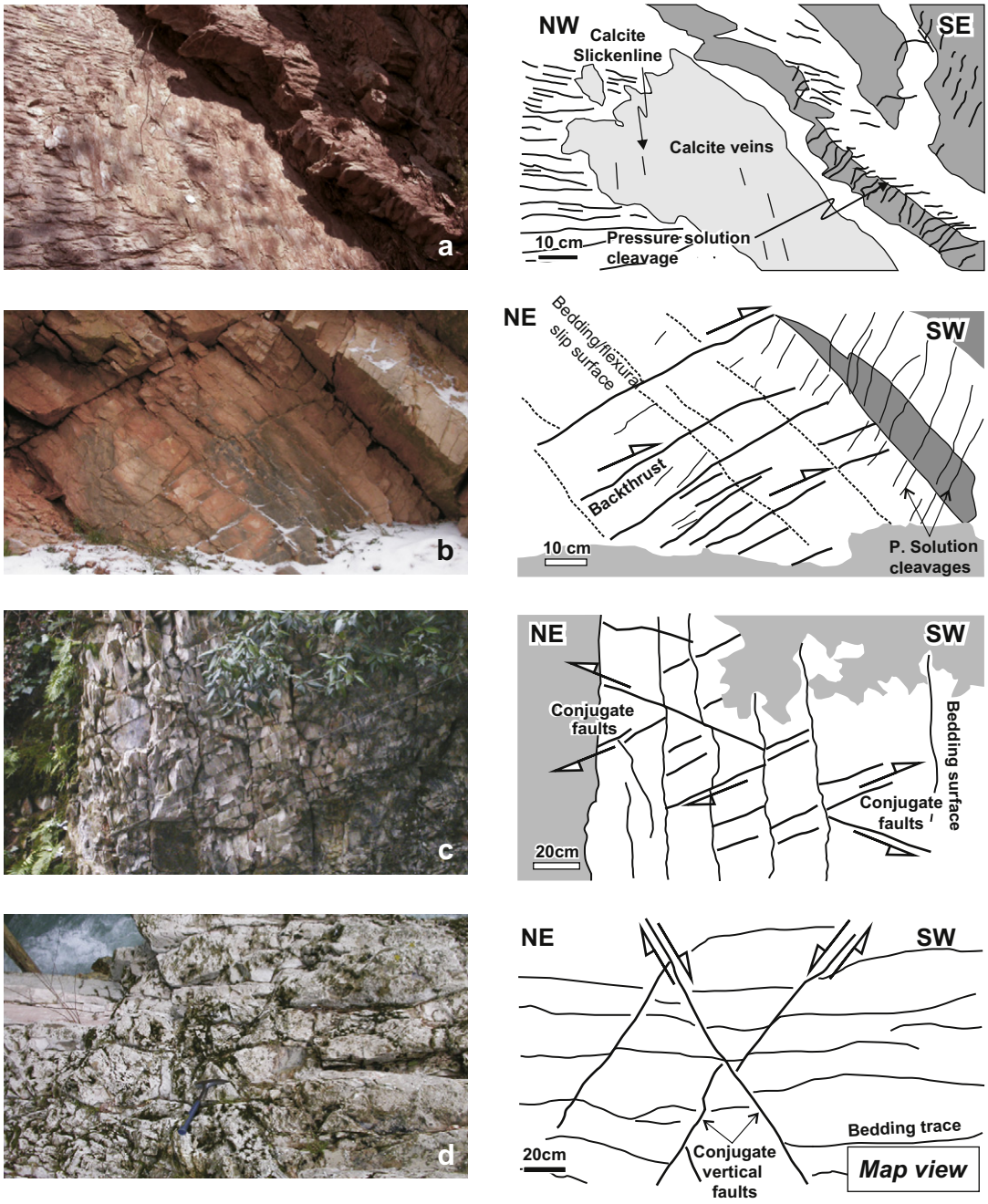

Fig. 4. Example of structural cross-cutting relationships. (a) Layer-parallel slip surfaces associated with pressure solution cleavages at a high angle to bedding in the backlimb of the Mt. Catria anticline (*Scaglia* formation). (b) Hinterland-verging small-scale reverse faults overprinting pressure solution cleavages at a high angle to bedding in the backlimb of the Mt. Catria anticline (*Scaglia* formation). (c) Thrusts and layer-parallel cleavages and (d) conjugated strike–slip faults overprinting pressure solution cleavage at a high angle to bedding in the forelimb of the Mt. Catria anticline (*Scaglia* formation).

0° (Fig. 7f). The orientation of the corresponding slickenlines in the unrotated and in the rotated space indicates that many of these faults can be interpreted as belonging to two reverse conjugate subsets having a σ_1 trending NE–SW parallel to bedding (subset VI a) and horizontal (subset VI b), respectively (Fig. 7g). Subset VII includes faults that in their present orientation define a conjugate strike–slip system compatible with a NE–SW shortening direction (i.e. parallel to the transport direction) (Fig. 7h).

3.2. Fracture data (joint, vein and generic fracture)

Fractures occur in all the mechanical units exposed in the Mt. Catria anticline. Their length ranges from few millimetres to several meters, and are both stratabound and, mostly in the *Calcare Massiccio* Formation, unstratabound (Fig. 5a). They aperture is mostly lower than 0.5–1 mm (Fig. 5b,c). These deformation structures are generally not constantly spaced, particularly in the *Scaglia* and *Maiolica* Formations, where

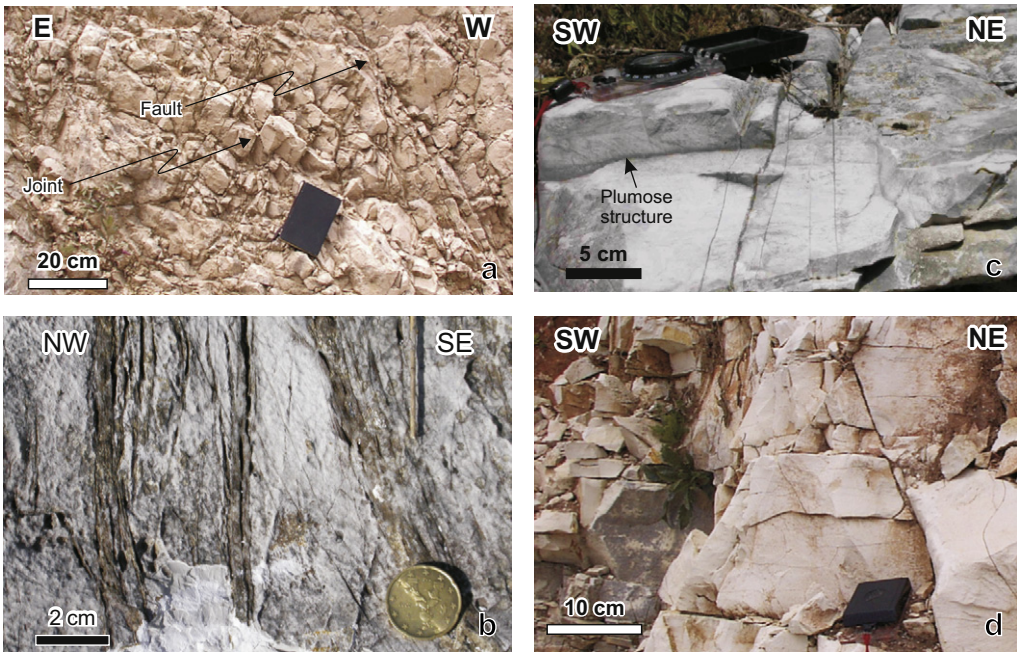

Fig. 5. (a) Unstratabound joints and faults in the crestal sector of the Mt. Catria anticline (*Calcare Massiccio* formation). (b) Example of vein array in the *Maiolica* Formation. Hairline veins represent the most part of extensional structure in the *Maiolica* and *Scaglia* Formations. (c) Longitudinal veins and transverse joint with plumose structures in the crestal sector of the anticline (*Maiolica* Formation). In the longitudinal array, only one vein allows recognition of its tensile origin, the others are classified as uncertain veins they parallel to an element of certain attribution. (d) Longitudinal normal faults in the crestal sector of the Mt. Catria anticline (*Scaglia* Formation). The mesostructural associations are also used to interpret the fracture subsets. In this case, this structure supported the interpretation of longitudinal generic fractures as joint/vein.

they are mostly filled by calcite. In the *Corniola* and *Calcare Massiccio* Formations calcite veins are rare. Fracture data includes: 239 veins that allowed to recognise an opening direction about perpendicular to the fracture walls, 25 joints which exhibit plumose structures, 107 uncertain joints/veins, and 381 generic fractures (e.g. isolated veins with small aperture not sufficient to exclude a shear component during the opening; isolated weathered fractures).

Poles to fractures, show a dominant set striking at a high angle to the fold axis, i.e. transverse (e.g. Stearns, 1968; Hancock, 1985), and a subordered set striking parallel to the fold axis, i.e. longitudinal (Stearns, 1968), both in their present orientation and after bed rotation, (Fig. 9a). Fracture dip is about 90° both in the rotated and unrotated analysis. Decreasing of standard deviation in the rotated fracture dip analysis supports the use of the rotated dataset to analyse and classify fractures. Azimuth data are characterised by a polymodal distribution that we interpret as the sum of N independent Gaussian distributions. Accordingly, the fracture azimuthal dataset can be divided into five subsets (Fig. 9b):

- Subset I includes joints, veins and generic fractures striking sub parallel to the fold axis trend (azimuth is N128°E ± 12°) and about perpendicular to bedding (ATB is 89° ± 9°; ATB is lower than 90° when surfaces dip toward the north). These fractures correspond to Type 2 fracture of Stearns (1968). In most cases, this set exhibits a tensile origin (Fig. 9b), consistent with other mesostructures indicating hinge perpendicular extension (Fig. 5d). Generic fractures of this subset were therefore included in the joint/vein dataset.
- Subset II includes joints, veins and generic fractures striking N31°E (±20°) (ATB is 91° ± 6°).
- Subset III mostly includes element of uncertain attribution striking N64°E (±7°) (ATB is 90° ± 8°).

Fracture subsets striking N31°E and N64°E are likewise interpreted as an asymmetric Type I fracture array of Stearns (1968). This fracture array, commonly associated to thrust-related anticlines, includes a joint/vein set bisecting two conjugate fault sets (e.g. Stearns, 1968; Hancock, 1985; Price and Cosgrove, 1990; Cooper, 1992; among the others). Accordingly, subset II includes transverse joints and veins; subset III includes left-lateral faults. This interpretation is confirmed by the occurrence of joints and veins striking perpendicular to the fold axis (Fig 9b) and left-lateral faults striking sub-parallel to N64°E striking subsets (Fig. 7c). In this interpretation, the Type I fracture set is asymmetrical, because the right-lateral fault system does not occur. Accordingly, transverse generic fractures of subset II are included in the joint/vein dataset, and those of subset III are included in the left-lateral fault dataset.

- Subset IV includes mostly generic fractures striking N162°E (±11°) and perpendicular to bedding (ATB is 91° ± 8°).
- Subset V includes generic fractures striking N88°E (±10°) and perpendicular to bedding (ATB is 90° ± 9°).

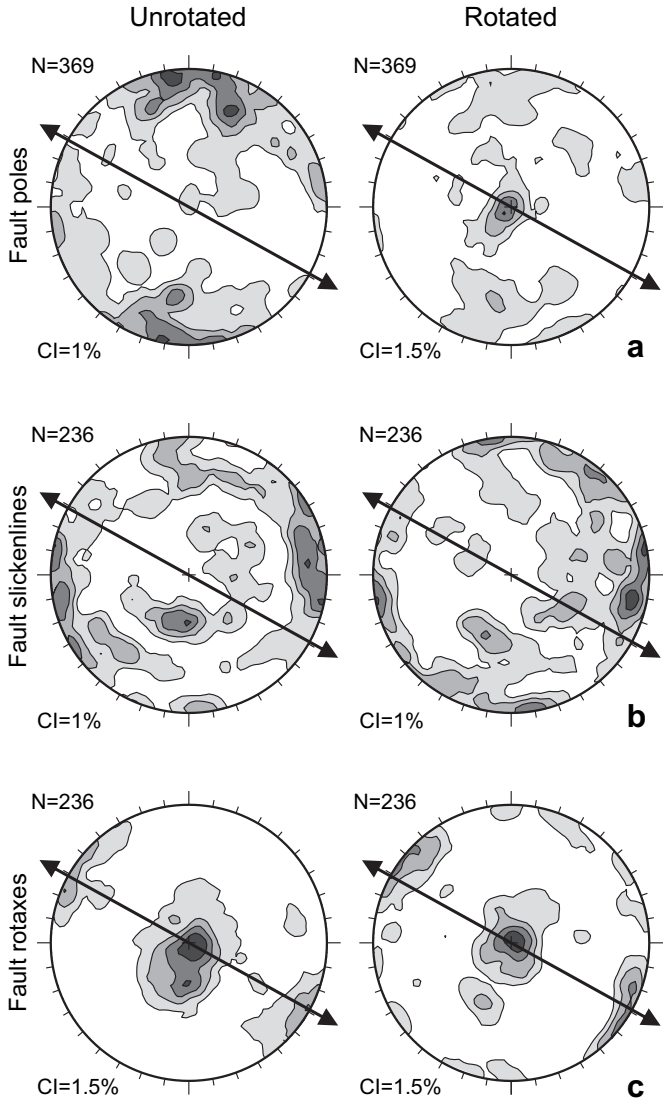

Fig. 6. Cumulative faults analysis with reference frame of unrotated and rotated bedding. Contouring of (a) poles to fault, (b) fault slickenlines, and (c) fault rotaxes. Black arrows indicate the fold axial trend.

Fracture subsets IV and V do not include elements of certain attribution and are sub parallel to fault subsets I (slickenlines strike N167°E ± 7°) and III (slickenlines strike N79°E ± 7°). Due to their uncertain attribution, these structures were not included in the joint/vein dataset.

3.3. Pressure solution cleavage data

Solution cleavages are stratabound undulatory surfaces, mainly developed in the *Maiolica* and *Scaglia* Formations. The comparison between rotated and unrotated contouring on equal-area stereonets and the dip frequency distribution (Fig. 10a) highlight that these deformation structures are at a high angle to bedding and define a single set striking N123° (±15°), i.e. parallel to the fold axis trend (longitudinal cleavage; Fig. 10b). Cleavage spacing relates to the corresponding bed thickness (Fig. 11), supporting the use of the normalised spacing of solution cleavage (*H/S* ratio) to compare deformation intensities between different fold sectors (e.g. Sans et al., 2003; Tavani et al., 2004, 2006a). In some cases, the tectonic pressure solution cleavages terminate against bedding-parallel pressure solution cleavages. To provide results not influenced by possible reactivation of the bedding-parallel cleavage, these few data were not included in the H/S analysis.

3.4. Cross-cutting relationships

Cross-cutting relationships between the different mesostructure sets were observed in the field. Layer-parallel slip surfaces are associated with pressure solution cleavages at a high angle to bedding (Fig. 4a). In the backlimb of the anticline, these elements are overprinted by hinterland-verging, small-scale reverse faults belonging to the fault set VIb (Fig. 4b). In the forelimb, conjugate reverse faults belonging to set VIb and strike–slip faults belonging to set VII developed contemporary to pressure solution cleavages parallel to bedding, as attested by their mutual cross-cutting relationships (Fig. 4c,d). Pre-existing, compaction-related bedding-parallel pressure solution surfaces in the forelimb were reactivated at this stage. Thrusts, strike–slip faults, and layer-parallel cleavages overprint pressure solution cleavage at a high angle to bedding (coeval to layer-parallel slip surfaces) (Fig. 4c). It is worth noting that these conjugate fault pairs in the forelimb developed with the maximum principal stress axis σ_1 subhorizontal and perpendicular to the fold axis, while the intermediate principal stress axis σ_2 is both near horizontal (Fig. 4c) and near vertical (Fig. 4d), indicating that an inversion between σ_2 and σ_3 has occurred. Relationships between these faults sets cannot be established in the field, because they locate at different sites. Longitudinal pressure solution cleavages at a high angle to bedding are coeval with transverse joints/veins, as indicated by their mutual cross-cutting relationships.

4. Identification of synfolding structures

Analysis of mesostructure attributes and of the variability of these attributes across the fold strike allowed us to constrain the relative timing between mesostructures development and folding (e.g. Harris and Van Der Pluijm, 1998; Bellahsen et al., 2006; Tavani et al., 2006a). In particular, deformation structures are classified as syn-folding *sensu latu* if they developed in the period spanning from blind thrust propagation and negligible folding, to late stage fold tightening; structures are classified as syn-folding *sensu strictu* if they developed during fold amplification (Tavani et al., 2006a).

4.1. Pressure solution cleavage

We investigated the spatial distribution of cleavage attributes in the *Maiolica* Formation. Fig. 12b illustrates the across-strike variability of solution cleavage angle to bedding. This parameter is scattered about the average value of 90.5° (±32.0°) across the anticline. Cleavage frequency, computed

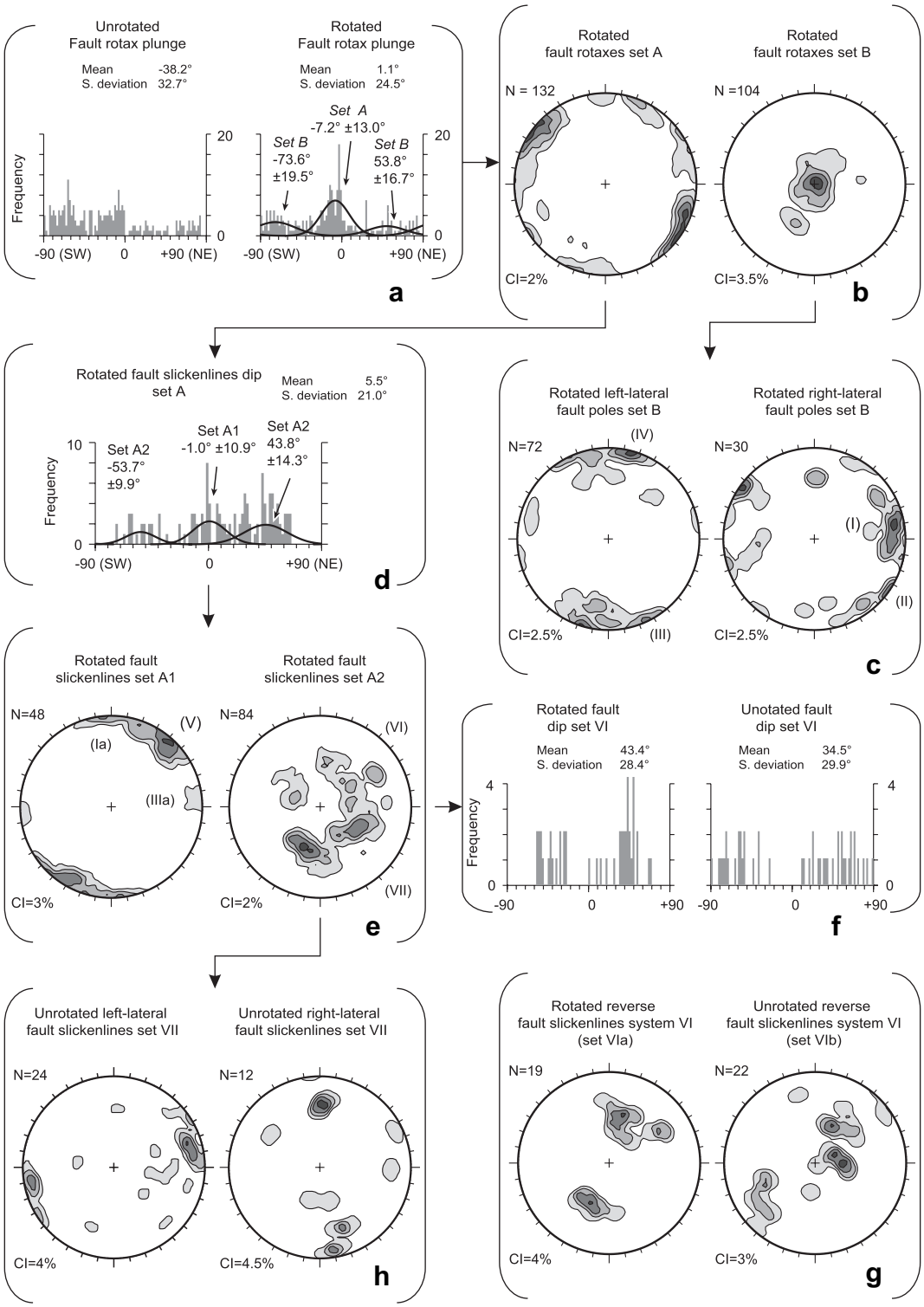

Fig. 7. Faults analysis and classification. See text for details.

as H/S, shows a progressive decrease from both the backlimb and forelimb toward the crest (Fig. 12c). This strong correlation between structural position and cleavage frequency, coupled with the observation that this deformation structure strikes parallel to the fold axis trend, suggests that pressure solution cleavages in the Mt. Catria anticline have a syn-folding *sensu strictu* origin (e.g. Tavani et al., 2006a).

4.2. Joints and veins

We examined the spatial distribution of joint/vein attributes in the *Maiolica* Formation (Fig. 12d). The azimuthal analysis illustrates that joints and veins are both longitudinal and, mainly, transverse to the fold axial trend. In particular, the longitudinal set localises mostly in the fold crest. This across

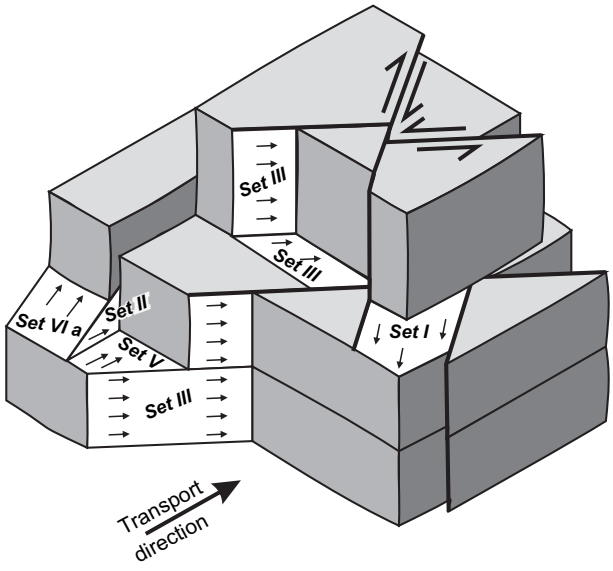

Fig. 8. Schematic illustration of fault subsets geometry.

strike variability, coupled with the observation that joints and veins are coeval with the pressure solution cleavage, allowed us to interpret that they developed at least partially during fold amplification (i.e. syn-folding *sensu strictu*).

4.3. Faults

The unfolded slickenline bearing of fault subsets II and V (N32°E ± 8°) is perpendicular to the fold axis trend, as well as the unfolded slickenline bearing of fault subset VIa (N25°E ± 11°) (Figs. 7 and 8). The slickenline bearing of subset VIb (N38°E ± 18°; in the unrotated analysis) is also perpendicular to the fold axis trend. Conjugate strike–slip faults belonging to subset VII have an acute bisector trending in the unrotated analysis N35°E, compatible with those of the other subsets. It follows that fault data belonging to all these subsets are consistent with a σ_1 trending parallel to the transport direction. Accordingly, these fault subsets are interpreted as syn-folding *sensu latu*.

Fault subsets I and III form a conjugate strike–slip system compatible with the tectonic transport direction (Fig. 8) because their slikenline bisectors (N33°E and N123°E) are orthogonal and parallel to the trend of the fold axis in the study area (N119°). This conjugate subset has a dihedral angle of about 90°, as first described in this region by Marshak et al. (1982). According to these authors, this high dihedral angle indicates that these faults could be pre-folding extensional structures reactivated as faults during folding. This hypothesis could be supported by the occurrence of generic fracture sets striking N162°E and N88°E, that we have grouped with fault subsets I and III. The lack of good kinematic data on these fractures makes our grouping equivocal, however, and in the following analysis we only discuss information related to their syn-folding activity (i.e. slickenlines and rotaxes of fault belonging to subsets I and III).

Fig. 12e,f shows the across-strike variability of the slickenline and rotax plunge for fault subsets I to V and VIa,

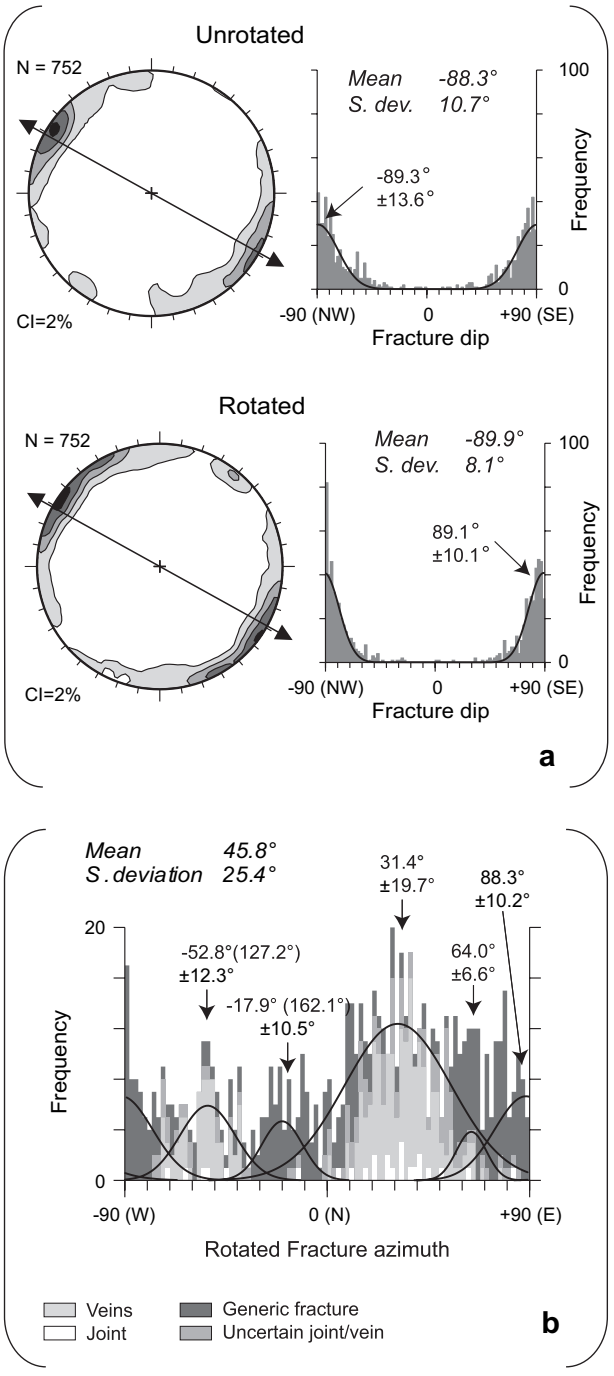

Fig. 9. Fracture cumulative analysis. (a) Contouring of total poles to fracture and dip frequency analysis and Gaussian best fit, with reference frame of unrotated and rotated bedding. (b) Frequency analysis and Gaussian best fit of fractures azimuth.

respectively. Slickenlines are mostly sub parallel to the corresponding bedding surfaces, particularly in the crestal zone. Few faults with slickenlines oblique to bedding localise in the fold limbs. The rotated rotax plunge progressively passes from 0° in the backlimb, to 90° in the crestal sector, and to 0° again in the forelimb sector, where the transition to the crest is rather abrupt. Faults belonging to subsets VIb and VII occur in the backlimb and, mostly, in the forelimb of the Mt. Catria anticline. This correspondence between fault

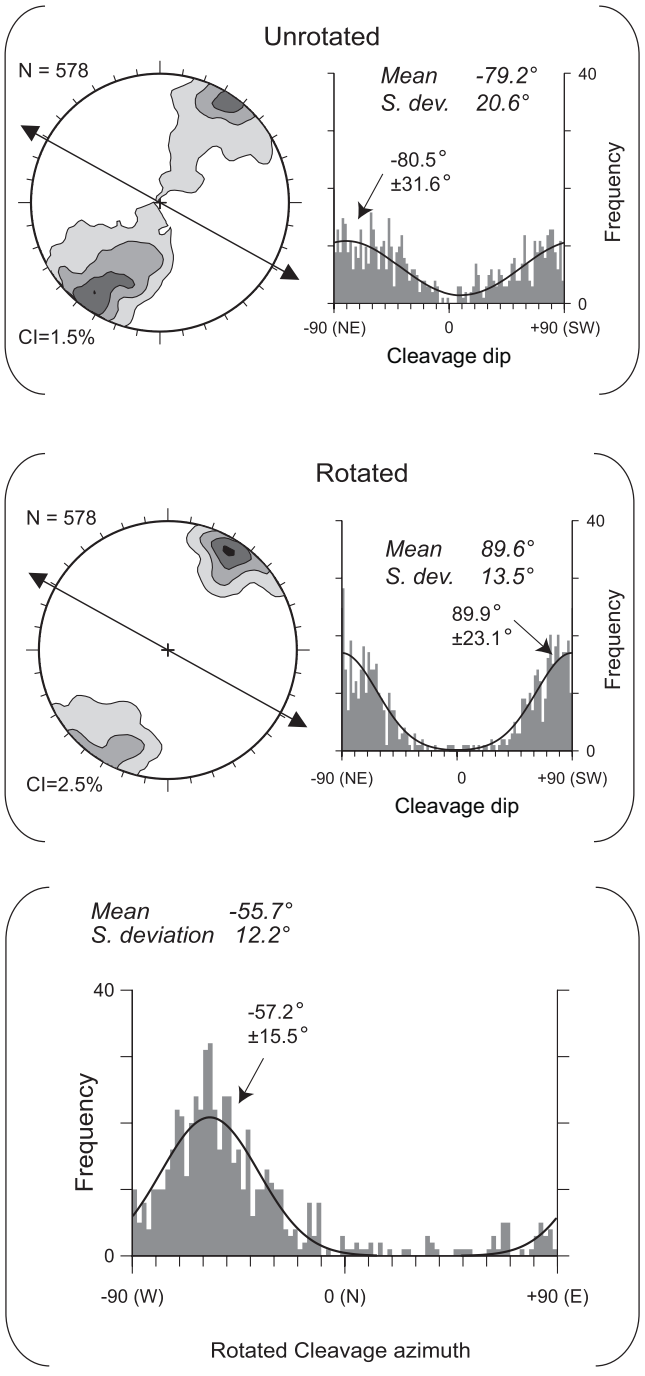

Fig. 10. Cumulative analysis of pressure solution cleavages. (a) Contouring of total poles to pressure solution cleavages and dip frequency analysis and Gaussian best, with reference frame of unrotated and rotated bedding. (b) Frequency analysis and Gaussian best fit of pressure solution cleavages azimuth.

attributes and structural position confirms that these fault subsets developed during fold amplification (i.e. they are at least partially syn-folding *sensu strictu*).

4.4. Across-strike variability and structural control on deformation pattern

By analysing the spatial distribution of fault kinematics (e.g. Rocher et al., 2000; Anastasio and Holl, 2001; Silliphant et al., 2002) and the attributes of solution cleavages and joints/veins in the *Maiolica* Formation, we related the deformation pattern to the structural position. In particular, analysis of the spatial variability of the attributes of syn-folding deformation structures allowed the recognition of three fold sectors characterised by a roughly homogeneous deformation pattern. Mesofault, cleavage, and joint/vein attributes have a spatial variability that relates to the structural position within the anticline. These attributes vary systematically across the fold trend, following the progressive variation of bedding dip. As a consequence, the boundaries of these sectors are not well defined and roughly coincide with the backlimb, the crest, and the forelimb (Fig. 12).

4.5. Layer-orthogonal variability

Solution cleavage and joint/vein data from all the lithologies were used to analyse the variability of deformation patterns within fold sectors, as a consequence of the variable mechanical stratigraphy in the folded multilayer (e.g. Fischer and Jackson, 1999). The stratigraphic control on the deformation pattern is investigated through stratigraphic transects perpendicular to bedding in the backlimb (*Scaglia*, *Maiolica*, and *Corniola* Formations) and in the crest (*Maiolica*, *Corniola*, and *Calcare Massiccio* Formations) (Fig. 13). The cleavage ATB is rather scattered and the average value is about 90°, regardless of the lithology. The cleavage frequency (H/S) in the *Scaglia* Formation is high in the uppermost part, and decreases with the depth. Such behaviour relates to the presence of a regional thrust in the basal part of the overlying *Scaglia Cinerea* Formation whose influence decreases with the depth. Cleavage H/S values in the lower part of the *Scaglia* Formation, in the backlimb, are similar to those of the *Maiolica* Formation, with an average value near 2 in the upper part of the folded multilayer (i.e. *Scaglia* and *Maiolica* Formations). Pressure solution cleavages are rare in the *Corniola* and *Calcare Massiccio* Formations, where joints (and subordinately veins) and small-scale faults occur. Joints and veins are both longitudinal and transverse. In the backlimb of the Mt. Catria anticline, longitudinal joints/veins rarely occur and mostly locate in the lower part of the multilayer (i.e. in the *Corniola* Formation). In the fold crest, longitudinal and transverse joints and veins occur in the *Maiolica*, *Corniola*, and *Calcare Massiccio* Formations. The last two transects illustrate the stratigraphic control on the fault rotax plunge (rotated analysis) in the backlimb and in the crest of the anticline. They show that, as observed in the across strike transect, the backlimb is mostly characterised by rotaxes at a low angle to bedding, regardless of the lithology. The crest is characterised by rotaxes that are mostly at a high angle to bedding, regardless of the lithology.

It has to be emphasised that in the *Calcare Massiccio* Formation, faults and joints are unstratabound, pervasive deformation structures. Conversely in the other formations these structures mostly terminate at bedding surfaces. It follows that, in the overlying formations folding is facilitated by flexural-slip (as also testified by the occurrence of flexural-slip surfaces), whereas in the *Calcare Massiccio* Formation,

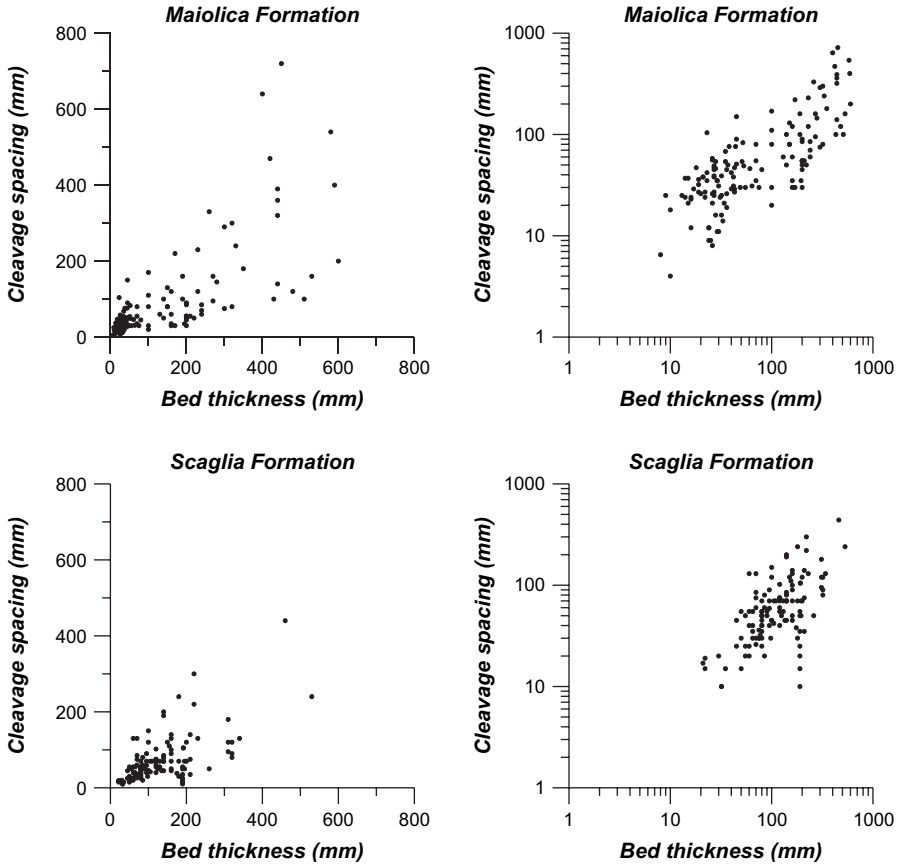

Fig. 11. Pressure solution cleavage H/S scattergrams in the normal and log–log spaces for the *Scaglia* and *Maiolica* Formations.

cataclastic flow (e.g. Stearns, 1978; Ismat and Mitra, 2001) is an important deformation mechanism.

4.6. Structural summary

The distribution of deformation structures in the Mt. Catria anticline and their overprinting relationships are schematically summarised in Fig. 14. Flexural slip and rotated dip–slip faults localise in the backlimb and in the forelimb, both in the *Maiolica* and in the *Scaglia* Formation. In these sectors, late stage reverse and strike–slip faults occur, associated with a sub-horizontal σ_1 trending perpendicular to the fold axis. In the crestal sector, in the *Maiolica*, in the *Corniola*, and in the *Calcare Massiccio* Formations, mesofaults include conjugate strike–slip faults with a 90° dihedral angle, associated with a σ_1 parallel to bedding and trending perpendicular to the fold axis. Small-scale faults without evidence of slip are interpreted as to Type I fractures of Stearns (1968), and include the left-lateral system. These features occur throughout the entire fold.

Joints and veins in the Mt. Catria anticline include elements whose height, in the *Scaglia*, *Maiolica* and *Corniola* Formations range from few centimetres to stratabound, whereas in the *Calcare Massiccio* Formation these elements mostly cut across the poorly defined bedding surfaces. Transverse joints and veins occur in all the formations and in all the structural positions. Longitudinal joints and veins localise mostly in the crestal fold sector. The *Scaglia* and *Maiolica* Formations include mostly veins, whereas in the *Corniola* and *Calcare Massiccio* Formations mostly comprise joints.

Longitudinal stratabound solution cleavage at a high angle to bedding is the most pervasive and well-organised structure in the uppermost sectors of the multilayer. This deformation structure is coeval with transverse tensile structures, left-lateral faults belonging to Type I of Stearns (1968), and with both flexural-slip and rotated dip–slip faults (i.e. they are syn-folding). Cleavage frequency decreases from the fold limbs toward the crestal sector, where its occurrence, in the *Maiolica* Formation, is negligible. In the lower multilayer sector, the occurrence of longitudinal stratabound solution cleavage is negligible.

5. Discussion

5.1. Timing of deformation structures

Analysis of the deformation pattern in the Mt. Catria anticline shows that both the attitude and kinematics of most deformation structures are consistent with a stress field whose principal axes are: (1) the axis perpendicular to the bedding surface; (2) the fold axis trend; (3) the axis lying on the bedding surface and perpendicular to the fold axis trend.

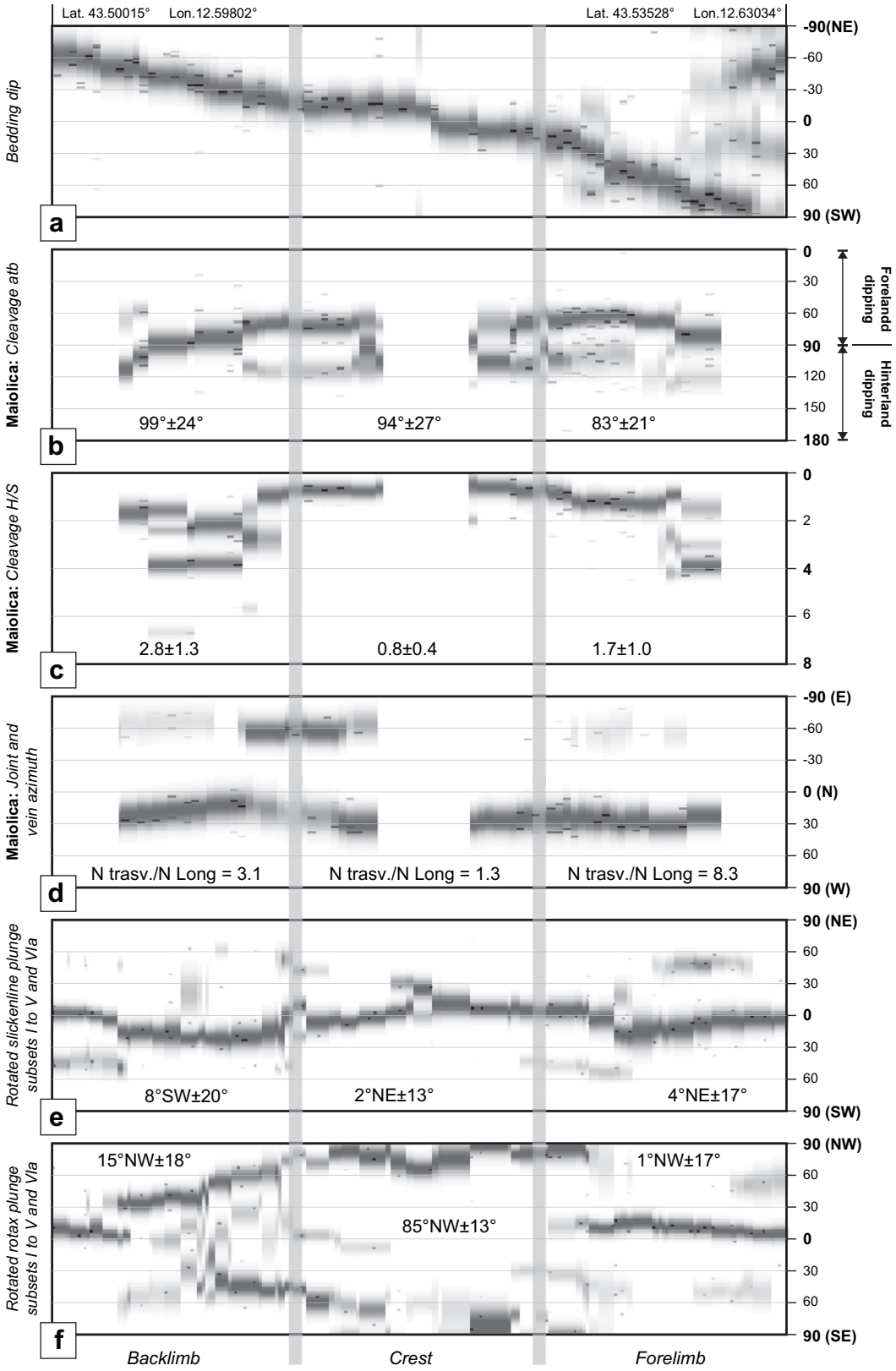

Fig. 12. Structural transects across the fold strike. See text for details and Fig. 2 for location. Average value and standard deviation of the considered parameter in the fold sector are reported. For the joint/vein azimuth analysis, the ratio between transverse and longitudinal elements is reported.

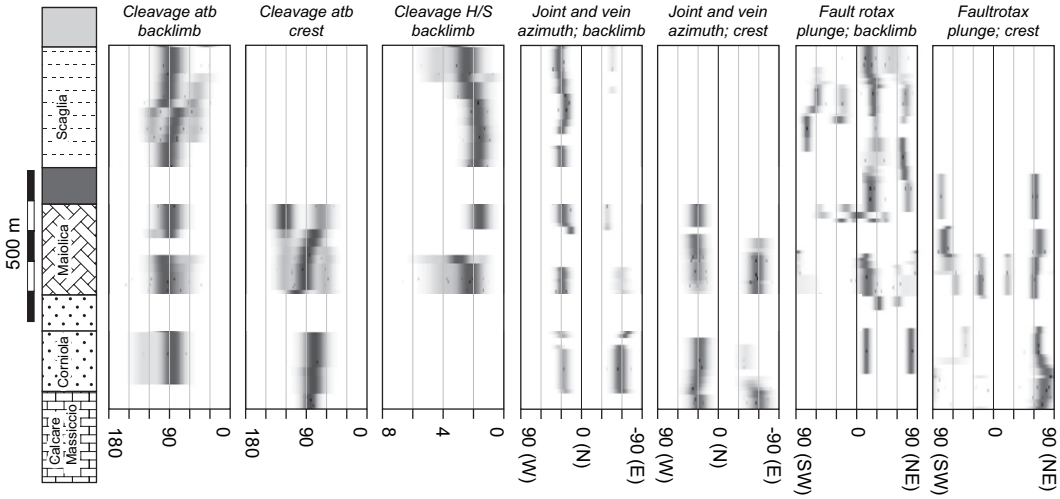

Fig. 13. Stratigraphic transects in the backlimb and in the crest of the Mt. Catria anticline.

This supports our interpretation that these structures have a syn-folding *sensu latu* origin (e.g. Price, 1966). In particular, pressure solution cleavage at a high angle to bedding is the most pervasive and well-organised element and strongly correlates with the structural position. Type I fractures that include transverse joints/veins and left-lateral small scale faults, accommodate an along axis elongation commonly recognised in fold-and-thrust belts (e.g. Hossack, 1979; Kilsdonk and Wiltschko, 1988; Price and Cosgrove, 1990; Srivastava and Engelder, 1990; Ferrill and Groshong, 1993; Lemiszki et al., 1994; Gutiérrez-Alonso and Gross, 1999), but do not exhibit univocal cross-cutting relationships with the syn-folding solution cleavage. Accordingly, we interpret these elements as early-stage (e.g. Price and Cosgrove, 1990) to syn-folding (e.g. Srivastava and Engelder, 1990), because they started to develop very early in the folding process, and continued during fold amplification.

In the *Maiolica* Formation, the occurrence of longitudinal joints/veins in the crestal sector, where lower cleavage intensity is observed, indicates that a progressive decreasing of the σ_1 magnitude has occurred, up to the inversion between σ_1 and σ_3. Such an inversion occurred during fold amplification. Few outcrops of the lower part of the *Scaglia* Formation in the crestal sector are also characterised by the occurrence of

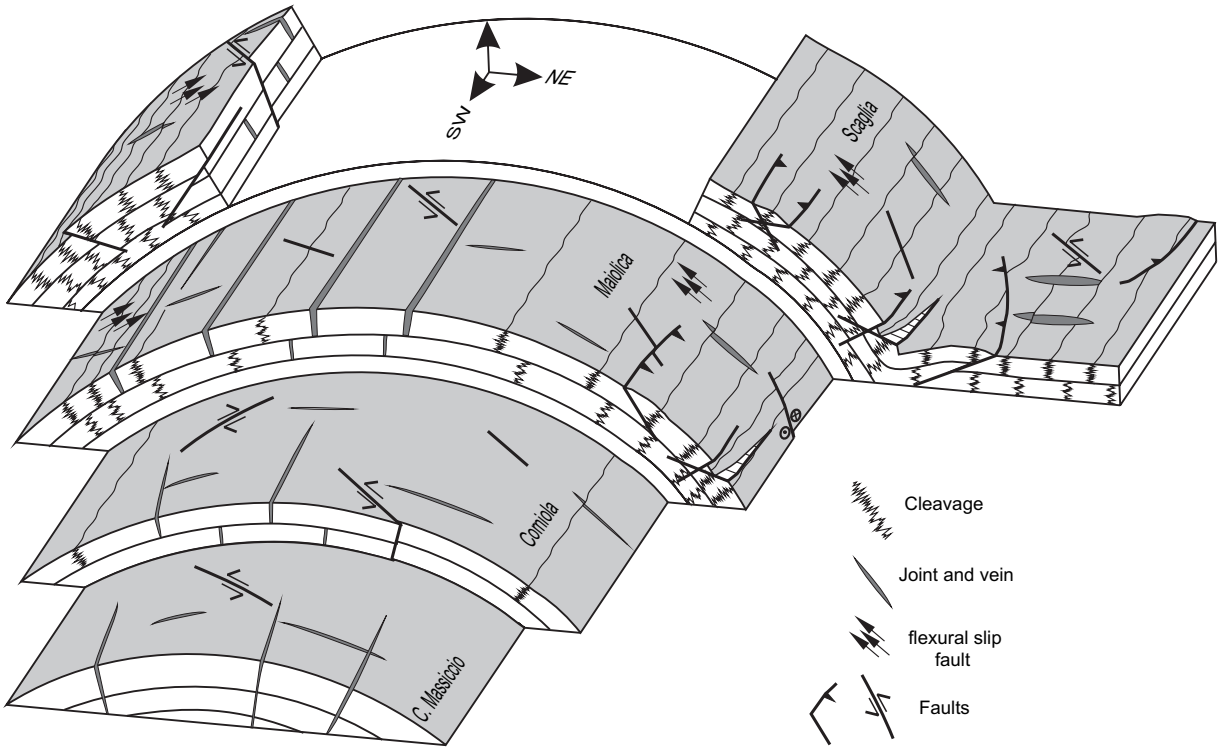

Fig. 14. Schematic illustration of the mesoscale structures' spatial distribution and of their cross-cutting relationships. See text for details.

longitudinal extensional features (Fig. 5d), thus confirming the occurrence of syn-folding hinge-normal extension.

Flexural slip, rotated dip–slip, and rotated strike–slip faults, have been interpreted also as syn-folding, because of the strong correlation between fault rotax/slickenline attributes and structural position. Accordingly, these faults are coeval with transverse tensile structures and longitudinal solution cleavages. The residual dataset mostly includes faults associated with a sub-horizontal maximum compressional axis parallel to the transport direction, and are associated with late-stage fold tightening (e.g. Ramsay, 1974; Allmendinger, 1982).

5.2. Stratigraphic versus structural control on deformation patterns

Analysis of the deformation pattern variability in the different formations showed that: (1) the *Scaglia* and the *Maiolica* Formations can be grouped into a single mechanical unit because they exhibit a very similar deformation pattern (i.e. similar solution cleavage ATB and H/S); (2) the *Corniola* Formation represents another mechanical unit, characterised by a decreased occurrence of the pressure solution cleavage; (3) the *Calcare Massiccio* Formation represents a third mechanical unit, with a deformation pattern similar to that of the *Corniola* Formation, although flexural-slip folding appears to dominate the *Corniola* Formation, whereas cataclastic flow predominates in the *Calcare Massiccio* Formation.

The different behaviour between the mechanical units 1 and 2 does not correspond to significant variations in the mechanical attributes of the multilayer. The *Corniola* and the *Maiolica* Formations are, in fact, more similar than the *Scaglia* and the *Maiolica* Formations. The *Scaglia* is characterised by a greater amount of clay content with respect to both the *Corniola* and the *Maiolica* Formations, which are also characterised by similar bed thickness, greater than that of the *Scaglia* Formation. The mechanical similarity between the *Corniola* and the *Maiolica* Formations, coupled with their different deformation patterns, suggests that deformation partitioning in these units was strongly influenced by different water circulation conditions (Engelder and Marshak, 1985): an open system in the upper part and a closed system in the lower part of the folded multilayer. Engelder and Marshak (1985) placed the *Maiolica* Formation in the close circulation system. In contrast, our data indicate that pressure solution cleavage is an important and pervasive element in the *Maiolica* Formation, therefore must have been deformed in an open system where the possibility for calcite removal enhanced the pressure solution process (e.g. Engelder and Marshak, 1985). Accordingly, we infer that the sealing level dividing the open and closed water circulation systems was represented by the *Bosso* Formation (Fig. 1).

5.3. Fold evolution

The analysis of deformation pattern distribution provides an additional tool for inferring the Mt. Catria anticline kinematic evolution (e.g. Salvini and Storti, 2001; Tavani et al., 2006a), which is illustrated in Fig. 15. The anticline initially grew by décollement folding. At this stage, the *Anidridi di Burano* Formation provided the ‘‘low competent’’ unit, the *Calcare Massiccio* Formation acted as the dominant member of the folded multilayer, which determined the dimensions and the geometry of the anticline (e.g. Biot, 1961), and the overlying formations deformed by flexural-slip folding. Fold progression lead to the progressive fold tightening and to the formation of two conjugated thrusts nucleated in the *Calcare Massiccio* and *Corniola* Formations (Fig. 15b). At this stage the fold internal architecture was that of an asymmetric faulted décollement anticline (e.g. Mitra, 2003). The folding progression by double-edge fault-propagation folding (Tavani et al., 2006b) caused the upward and downward propagation of the faults and the linkage between the frontal ramp and both the lower and the upper décollements. The shortening progression caused the partial translation of the anticline onto the upper décollement (Fig. 15c) and its final deformation by fault bend folding (e.g. Suppe, 1983).

The inferred kinematic evolution of the Mt. Catria anticline is consistent with the following evidence. (1) The deformation

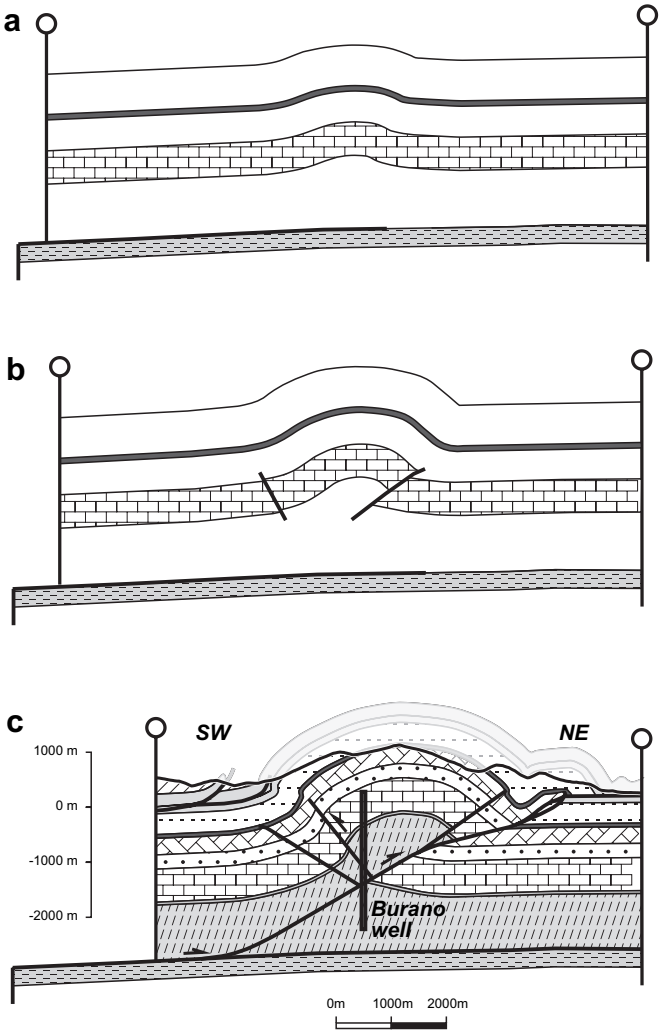

Fig. 15. Cartoon showing the kinematic evolution of the Mt. Catria anticline.

pattern mostly includes elements at a high angle to bedding, indicating that at the fold scale, in the exposed formations, no significant bed thinning/thickening has occurred during folding. (2) Flexural-slip surfaces are mainly located in the fold limbs, with a top to the crest shear sense in both the limbs, indicating that no significant excess shear (e.g. Mitra, 1992; Mosar and Suppe, 1992; Suppe et al., 2004) has occurred during folding. The presence all along the anticline of a backlimb sector dipping about 60° is consistent with the presence of a backthrust. (3) In décollement folding, the fold wavelength is dictated by the thickness of the competent unit (e.g. Currie et al., 1962). The observation, in the Mt. Catria anticline, that fold wavelength increases in those sector where the *Calcare Massiccio* formation exhibits an higher thickness (Fig. 1) supports the interpretation of the anticline as evolved, at least initially, by décollement folding. (4) The stratigraphic distribution of longitudinal solution cleavages allows the setting of constraints on the ramp nucleation. Its occurrence in the upper multilayer sector and its absence in the lower one are consistent with the growth of the anticline by double-edge fault-propagation folding (Tavani et al., 2006b). In this model, layer-parallel shortening occurs in those layers stratigraphically above the ramp upper tip initial stratigraphic elevation (Fig. 16). This would imply that, in the Mt. Catria anticline, the ramp has nucleated in the *Calcare Massiccio* and *Corniola* formations, and has propagated upward through the *Maiolica* and *Scaglia* formations. (5) The interpretation of the Mt. Catria anticline as a faulted décollement fold is also consistent with previous work (e.g. De Feyter and Menichetti, 1986; Barchi et al., 1991) and it is also supported by the observation that bedding dip in the Burano well progressively passes from about 10° in the shallower sectors, up to 70–75° in the deeper well sector (Martinis and Pieri, 1964), indicating disharmonic folding in the core of the anticline, as required by décollement folding (e.g. De Sitter, 1956).

6. Conclusions

Fold kinematics and mechanical stratigraphy played important roles in controlling the pattern of mesoscopic deformation in the Mt. Catria anticline. Our kinematic and geometric analysis of mesoscopic faults, joints, veins and solution cleavage suggests that, in a single mechanical unit, the fold can be divided in roughly homogeneously deformed sectors, corresponding to the backlimb, the crest and the forelimb. The variability of deformation pattern within each sector relates to the mechanical stratigraphy and to the environmental conditions of deformation (i.e. water circulation conditions).

In the Mt. Catria anticline, the exposed folded multilayer can be divided in three sectors: a first upper fractured and cleaved sector including the *Scaglia* and *Maiolica* Formations, a second fractured one, including the *Corniola* Formation, and a third sector including the *Calcare Massiccio* Formation. In the first two sectors, folding occurred by flexural slip whereas in the third lower sector, folding occurred by cataclastic flow. Partitioning between the first two sectors relates to thrust ramp nucleation and to the presence of a sealing unit dividing these sectors, which imposed different water circulation conditions. In the upper sector, the system was open and the pressure solution process was enhanced; in the lower sectors the system was closed and the possibility for pressure solution cleavage development was reduced.

The analysis of mesoscopic deformation patterns was a crucial undertaking that led to our unravelling the evolution of the Mt. Catria anticline. This evolution includes an early stage of décollement folding, followed by pop-up, double-edge fault-propagation folding. In the latest stages of fold growth, the hangingwall material was translated onto the upper décollement and deformed by fault-bend folding.

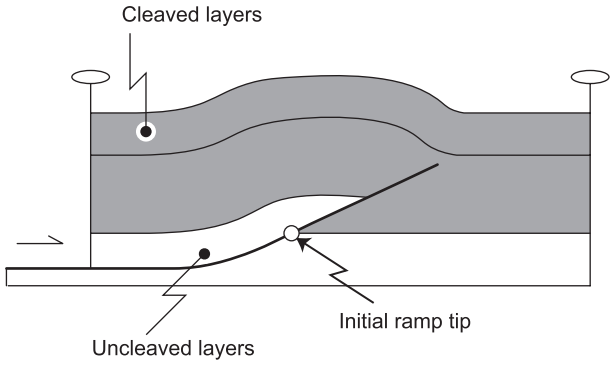

Fig. 16. Pressure solution cleavage stratigraphic distribution associated with double-edge fault-propagation folding.

Acknowledgements

We gratefully acknowledge constructive reviews from M.P. Fischer and N. De Paola, which helped us to improve an early version of the manuscript. This work was carried out with the financial support of the former Enterprise Oil Ltd, the Italian MIUR (Ministero dell'Università e della Ricerca), the MODES-4D (CGL2007-66431-C02-02/BTE) project, and the "Grup de Recerca de Geodinàmica i Anàlisi de Conques" (2001SRG-000074). We gratefully acknowledge ENI S.p.A. for their permission to publish the line drawing of a segment of line PS-338-85.

References

Allmendinger, R.W., 1982. Analysis of microstructures in the Meade plate of the Idaho–Wyoming foreland thrust belt U.S.A. Tectonophysics 85, 21–251.

Alvarez, W., 1989. Evolution of the Monte Nerone seamount in the Umbria-Marche Apennines: 1, Tectonic control of the seamount-basin transition. Bollettino della Società Geologica Italiana 108, 23–29.

Alvarez, W., Engelder, T., Geiser, P., 1978. Classification of solution cleavage in pelagic limestones. Geology 6, 263–266.

Anastasio, D.J., Holl, J.E., 2001. Transverse fold evolution in the External Sierra, southern Pyrenees, Spain. Journal of Structural Geology 23, 379–392.

Anelli, L., Gorza, M., Pieri, M., Riva, M., 1994. Subsurface well data in the Northern Apennines. Memorie della Società Geologica Italiana 48, 461–471.

Bally, A.W., Burbi, L., Cooper, C., Ghelardoni, R., 1986. Balanced cross section and seismic reflection profiles across the central Apennines. Memorie della Società Geologica Italiana 35, 257–310.

Barchi, M., Lavecchia, G., Menichetti, M., Minelli, G., Pialli, G., Nardon, S., 1991. Analisi della fratturazione del Calcare Massiccio in una struttura anticlinalica dell'Appennino umbro-marchigiano. Bollettino della Società Geologica Italiana 110, 101–124.

Bellahsen, N., Fiore, P., Pollard, D.D., 2006. The role of fractures in the structural interpretation of Sheep Mountain Anticline, Wyoming. Journal of Structural Geology 28, 850–867.

Bigi, G., Cosentino, D., Parlotto, M., Sartori, R., Scandone, P. (Eds.), 1989. Structural model of Italy 1:500.000. P.F.G. Quaderni della Ricerca Scientifica CNR, 114.

Biot, M.A., 1961. Theory of folding of stratified viscoelastic media and its implication in tectonics and orogenesis. Geological Society of America Bulletin 72, 1595–1620.

Calamita, F., Cello, G., Centamore, E., Deiana, G., Micarelli, A., Paltrineri, W., Ridolfi, M., 1991. Stile deformativo e cronologia della deformazione lungo tre sezioni bilanciate dall'Appennino umbro-marchigiano alla costa adriatica. Studi Geologici Camerti 1, 295–314.

Cardozo, N., Allmendinger, R.W., Morgan, J.K., 2005. Influence of mechanical stratigraphy and initial stress state on the formation of two fault propagation folds. Journal of Structural Geology 27, 1954–1972.

Centamore, E., Jacobacci, A., Malferrari, N., Martelli, G., Pieruccini, U., 1972. Carta Geologica d'Italia alla scala 1:50.000, F° 290 Cagli. Servizio Geologico D'Italia.

Centamore, E., Jacobacci, A., Malferrari, N., Martelli, G., Pieruccini, U., Valletta, M., 1975. Carta Geologica d'Italia alla scala 1:50.000, F° 291 Pergola. Servizio Geologico D'Italia.

Chamberlin, R.T., 1910. The Appalachian folds of central Pennsylvania. Journal of Geology 18, 228–251.

Chester, J.S., 2003. Mechanical stratigraphy and fault–fold interaction, Absaroka thrust sheet, Salt River Range, Wyoming. Journal of Structural Geology 25, 1171–1192.

Chester, J.S., Logan, J.M., Spang, J.H., 1991. Influence of layering and boundary conditions on fault-bend and fault-propagation folding. American Association of Petroleum Geologists Bulletin 103, 1059–1072.

Chilovi, C., De Feyter, A.J., Minelli, G., Barchi, M.R., 2002. Neogene strike–slip reactivation of Jurassic normal faults in the M. Nerone–M. Catria Anticline (Umbro-Marchean Apennines, Italy). Bollettino della Società Geologica Italiana 1, 199–207.

Cooper, M., 1992. The analysis of fracture systems in subsurface thrust structures from the foothills of the Canadian Rockies. In: McClay, K.R. (Ed.), Thrust Tectonics. Chapman and Hall, London, pp. 391–405.

Corbett, K., Friedmean, M., Spang, J., 1987. Fracture development and mechanical stratigraphy of Austin Chalk, Texas. American Association of Petroleum Geologists Bulletin 71, 17–28.

Couzens, B.A., Wiltschko, D.V., 1996. The control of mechanical stratigraphy on the formation of triangle zones. Bulletin of Canadian Petroleum Geologists 44, 165–179.

Currie, J.B., Patnode, H.W., Trump, R.P., 1962. Developments of folds in sedimentary strata. Geological Society of America Bulletin 73, 655–674.

Dahlstrom, C.D.A., 1990. Geometric constraints derived from the law of conservation of volume and applied to evolutionary models for detachment folding. American Association of Petroleum Geologists Bulletin 74, 336–344.

De Feyter, A.J., Menichetti, M., 1986. Back thrusting in forelimb of rootless anticlines, with examples form the Umbro-Marchean Apennines (Italy). Memorie della Società Geologica Italiana 35, 357–370.

De Sitter, L.V., 1956. Structural Geology. McGraw-Hill, New York.

Di Naccio, D., Boncio, P., Cirilli, S., Casaglia, F., Morettini, E., Lavecchia, G., Brozzetti, F., 2005. Role of mechanical stratigraphy on fracture development in carbonate reservoirs: Insights from outcropping shallow water carbonates in the Umbria–Marche Apennines, Italy. Journal of Volcanology and Geothermal Research 148, 98–115.

Durney, D.W., Kisch, H.J., 1994. A field classification and intensity scale for first-generation cleavages. Journal of Australian Geology & Geophysics 15, 257–295.

Elter, P., Giglia, G., Tongiorgi, M., Trevisan, L., 1975. Tensional and compressional areas in the recent (Tortonian to present) evolution of the Northern Apennines. Bollettino di Geofisica Teorica e Applicata 17, 3–19.

Engelder, T., Marshak, S., 1985. Disjunctive cleavage formed at shallow depths in sedimentary rocks. Journal of Structural Geology 7, 327–342.

Erickson, S.G., Jamison, W.R., 1995. Viscous-plastic finite-element models of fault-bend folds. Journal of Structural Geology 17, 561–573.

Ferrill, D.A., Groshong, R.H., 1993. Kinematic model for the curvature of the northern Subalpine Chain, France. Journal of Structural Geology 15, 523–541.

Fischer, M.P., Jackson, P.B., 1999. Stratigraphic controls on deformation patterns in fault-related folds: a detachment fold example from the Sierra Madre Oriental, northeast Mexico. Journal of Structural Geology 21, 613–633.

Fischer, M.P., Woodward, N.B., Mitchell, M.M., 1992. The kinematics of break-thrust folds. Journal of Structural Geology 14, 451–460.

Fraser, R.D.B., Suzuki, E., 1966. Resolution of overlapping absorption bands by least squares procedures. Analytical Chemistry 38, 1770–1773.

Geiser, P.A., 1988. Mechanisms of thrust propagation: some examples and implications for the analysis of overthrust terranes. Journal of Structural Geology 10, 829–845.

Gholipour, A.M., 1998. Patterns and structural position of productive fractures in the Asmari reservoirs, Southwest Iran. Journal of Canadian Petroleum Technology 37, 44–50.

Gross, M.R., 1995. Fracture partitioning: failure mode as a function of lithology in the Monterey Formation of coastal California. Geological Society of America Bulletin 107, 779–792.

Gutiérrez-Alonso, G., Gross, M.R., 1999. Structures and mechanisms associated with development of a fold in the Cantabrian Zone thrust belt, NW Spain. Journal of Structural Geology 21, 653–670.

Hancock, P.L., 1985. Brittle microtectonics: principles and practice. Journal of Structural Geology 7, 437–457.

Harris, J.H., Van Der Pluijm, B.A., 1998. Relative timing of calcite twinning strain and fold-trust belt development; Hudson Valley fold-trust belt, New York, U.S.A. Journal of Structural Geology 20, 21–31.

Hedlund, C.A., Anastasio, D.J., Fisher, D.M., 1994. Kinematics of fault-related folding in a duplex, Lost River Range, Idaho, U.S.A. Journal of Structural Geology 16, 571–584.

Hossack, J.R., 1979. The use of balanced cross-sections in the calculation of orogenic contraction: A review. Journal of the Geological Society of London 136, 705–711.

Ismat, Z., Mitra, G., 2001. Folding by cataclastic flow at shallow crustal levels in the Canyon Range, Sevier orogenic belt, west-central Utah. Journal of Structural Geology 23, 355–378.

Jamison, W.R., 1992. Stress controls of fold thrust style. In: McClay, K.R. (Ed.), Thrust Tectonics. Chapman and Hall, London, pp. 155–164.

Kilsdonk, B., Wiltschko, D.V., 1988. Deformation mechanisms in the southeastern ramp region of the Pine Mountain block Tennessee. Geological Society of America Bulletin 100, 653–664.

Lemiszki, P.J., Landes, J.D., Hatcher Jr., R.D., 1994. Controls on hinge-parallel extension fracturing in single-layer tangential-longitudinal strain folds. Journal of Geophysical Research 99, 22,027–22,042.

Marchegiani, L., Bertotti, G., Cello, G., Deiana, G., Mazzoli, S., Tondi, E., 1999. Pre-orogenic tectonics in the Umbria–Marche sector of the Afro-Adriatic continental margin. Tectonophysics 315, 123–143.

Mardia, K.V., 1972. Statistics of Directional Data. Academic Press, New York, p. 357.

Marshak, S., Geiser, P.A., Alvarez, W., Engelder, T., 1982. Mesoscopic fault array of the northern Umbrian Apennine fold belt, Italy: Geometry of conjugate shear by pressure-solution slip. Geological Society of America Bulletin 93, 1013–1022.

Martinis, B., Pieri, M., 1964. Alcune notizie sulla Formazione evaporitica del Triassico superiore nell'Italia centrale e meridionale. Memorie della Società Geologica Italiana 4, 648–672.

Massoli, D., Koyi, H.A., Barchi, M.R., 2006. Structural evolution of a fold and thrust belt generated by multiple decollements: analogue models and natural examples from the Northern Apennines (Italy). Journal of Structural Geology 28, 185–199.

Menichetti, M., De Feyter, A.J., Corsi, M., 1991. Crop 03—Il tratto della Val Tiberina-Mare Adriatico. Sezione geologica e caratterizzazione tettonico-sedimentaria delle avanfosse della zona umbro-marchigiano-romagnola. Studi Geologici Camerti 1, 279–293.

Mitra, S., 1992. Balanced structural interpretations in fold and thrust belts. In: Mitra, S., Fisher, G.W. (Eds.), Structural Geology of Fold and Thrust Belts. John Hopkins University Press, pp. 53–57.

Mitra, S., 2003. A unified kinematic model for the evolution of detachment folds. Journal of Structural Geology 25, 1659–1673.

Mosar, J., Suppe, J., 1992. Role of shear in fault-propagation folding. In: McClay, K.R. (Ed.), Thrust Tectonics. Chapman and Hall, London, pp. 123–132.

Price, N.J., 1966. Fault and Joint Development in Brittle and Semi-Brittle Rocks. Pergamon Press, Oxford.

Price, N.J., Cosgrove, J.W., 1990. Analysis of Geological Structures. Cambridge University Press, Cambridge.

Protzman, G.M., Mitra, G., 1990. Strain fabric associated with the Meade thrust sheet: implications for cross-section balancing. Journal of Structural Geology 12, 403–417.

Ramsay, J.G., 1967. Folding and Fracturing of Rocks. McGraw-Hill, New York, 568 pp.

Ramsay, J.G., 1974. Development of chevron folds. Geological Society of America Bulletin 85, 1741–1754.

Rocher, M., Lacombe, O., Angelier, J., Deffontaines, X., Verdier, F., 2000. Cenozoic folding and faulting in the south Aquitaine basin (France): insights from combined structural and paleostress analysis. Journal of Structural Geology 22, 627–645.

Salvini, F., Storti, F., 2001. The distribution of deformation in parallel fault-related folds with migrating axial surfaces: comparison between fault-propagation and fault-bend folding. Journal of Structural Geology 23, 25–32.

Salvini, F., Storti, F., 2004. Active hinge folding-related deformation and its role in hydrocarbon exploration and development: insights from HCA modeling. In: McClay, K.R. (Ed.), Thrust Tectonics and Petroleum Systems. American Association of Petroleum Geologists Memoirs 82, pp. 453–472.

Salvini, F., Billi, A., Wise, D.U., 1999. Strike–slip fault-propagation cleavage in carbonate rocks: the Mattinata Fault Zone, Southern Apennines, Italy. Journal of Structural Geology 21, 1731–1749.

Sanderson, D.J., 1982. Models of strain variation in nappes and thrust sheets: a review. Tectonophisics 88, 201–233.

Sans, M., Vergés, J., Gomis, E., Parés, J.M., Schiattarella, M., Travé, A., Calvet, F., Santanach, P., Doulcet, A., 2003. Layer parallel shortening in salt-detached folds: constraint on cross-section restoration. Tectonophysics 372, 85–104.

Santantonio, M., 1993. Facies associations and evolution of pelagic carbonate platform/basin systems: examples from the Italian Jurassic. Sedimentology 40, 1039–1067.

Silliphant, L.J., Engelder, T., Gross, M.R., 2002. The state of stress in the limb of the Split Mountain anticline, Utah: constraints placed by transacted joints. Journal of Structural Geology 24, 155–172.

Srivastava, D.C., Engelder, T., 1990. Crack-propagation sequence and pore-fluid conditions during fault-bend folding in the Appalachian Valley and Ridge, central Pennsylvania. Geological Society of America Bulletin 102, 116–128.

Stearns, D.W., 1968. Certain aspect of fracture in naturally deformed rocks, in: Rieker, R.E. (Ed.), National Science Foundation Advanced Science Seminar in Rock Mechanics. Special report, Air Force Cambridge Research Laboratories, Bedford, MA, AD66993751, pp. 97–118.

Stearns, D.W., 1978. Faulting and forced folding in the Rocky Mountains foreland. In: Laramide Folding Associated with Basement Block Faulting in Western United States. GSA Memoir, 151, pp. 1–38.

Storti, F., Salvini, F., 1996. Progressive rollover fault-propagation folding: a possible kinematic mechanism to generate regional-scale recumbent folds in shallow foreland belts. American Association of Petroleum Geologist Bulletin 80, 174–193.

Storti, F., Rossetti, F., Läufer, A.L., Salvini, F., 2006. Consistent kinematic architecture in the damage zones of intraplate strike–slip fault systems in North Victoria Land, Antarctica and implications for fault zone evolution. Journal of Structural Geology 28, 50–63.

Strayer, L.M., Suppe, J., 2002. Out-of-plane motion of a thrust sheet during along strike propagation of a thrust ramp: a distinct-element approach. Journal of Structural Geology 24, 637–650.

Suppe, J., 1983. Geometry and kinematics of fault-bend folding. American Journal of Sciences 283, 684–721.

Suppe, J., Connors, C.D., Zhang, Y., 2004. Shear Fault-bend Folding. In: McClay, K.R. (Ed.), Thrust Tectonics and Petroleum Systems. American Association of Petroleum Geologists Memoirs 82, pp. 303–323.

Tavani, S., Louis, L., Souque, C., Robion, P., Salvini, F., Frizon de Lamotte, D., 2004. Folding related fracture pattern and physical properties of rocks in the Chaudrons ramp-related anticline (Corbie'res, France). In: Swennen, R., Roure, F., Granath, J. (Eds.), Deformation, Fluid Flow and Reservoir Appraisal in Foreland Fold and Thrust Belts. AAPG Hedberg Series 1, pp. 257–275.

Tavani, S., Storti, F., Fernández, O., Muñoz, J.A., Salvini, F., 2006a. 3-D deformation pattern analysis and evolution of the Añisclo anticline, southern Pyrenees. Journal of Structural Geology 28, 695–712.

Tavani, S., Storti, F., Salvini, F., 2006b. Double-edge fault-propagation folding: geometry and kinematics. Journal of Structural Geology 27, 19–35.

Thorbjornsen, K.L., Dunne, W.M., 1997. Origin of a thrust-related fold: geometric vs kinematic tests. Journal of Structural Geology 19, 303–319.

Van Dijk, J.P., Bello, M., Toscano, C., Bersani, A., Nardon, S., 2000. Tectonic model and three-dimensional fracture network analysis of Monte Alpi (southern Apennines). Tectonophysics 324, 203–237.

Wise, D.U., McCrory, T.A., 1982. A new method of fracture analysis: azimuth versus traverse distance plots. Geological Society of America Bulletin 93, 889–897.

Wise, D.U., Vincent, R.J., 1965. Rotation axis method for detecting conjugate planes in calcite petrofabric. American Journal of Science 263, 289–301.

Wise, D.U., Funiciello, R., Parotto, M., Salvini, F., 1985. Topographic lineament swarms: Clues to their origin from domain analysis of Italy. Geological Society of America Bulletin 96, 952–967.

Woodward, N.B., Rutherford Jr., E., 1989. Structural lithic units in external orogenic zones. Tectonophysics 158, 247–258.